ISSN (Print) 1226-1750
ISSN (Online) 2233-6656
Journal of Magnetics 31(1), 60-69 (2026) https://doi.org/10.4283/JMAG.2026.31.1.60

Systematic Parametric and Sensitivity Analysis of Permanent Magnet Synchronous Motor for Water Pump Application

Tae-Yeong Jun[1], Yu-Seop Park[1]*, and Hyeon-Jae Shin[2]

[1]Dept. of Electrical Engineering Korea National University of Transportation, Chungju 27469, Republic of Korea
[2]Korea Institute of Industrial Technology, Gimje 54325, Republic of Korea

(Received 28 December 2025, Received in final form 26 February 2026, Accepted 27 February 2026)

This paper proposes the design and evaluation method to decrease torque ripple for Surface mounted Permanent Magnet Synchronous Motor (SPMSM). SPMSM type was adopted because it has the advantage of high efficiency and convenience of control for water pump. The design proceeds based on designing a motor with reduced torque ripple and magnet volume compared to motor in reference, and this paper uses Finite Element Analysis (FEA) method to evaluate different kinds of rotor. Then, proceed with a design that shows the optimal torque ripple by adjusting the offset and angle.

Keywords : SPMSM, water pump, torque ripple, comparison

1. Introduction

Traditional mechanical water pump's speed is based on engine speed, so even under low load high speed conditions where flow is not high, they still require a lot of power and provide cooling capacity. Recently, awareness of global environmental problems attracts the EV industry [1, 2]. According to these trends, the use of PMSMs in various vehicle components has been steadily increasing, and this shift has also contributed to the widespread adoption of electronic water pumps. However, rare-earth magnet that adopted in PMSM is high cost and the price fluctuations are large [3]. Therefore, reducing the magnet cost in PM many studies have presented various types of magnet design [4]. As part of this effort, the reference researched interior type of PMSM for their water pump with reduce torque ripple [5]. In this paper, final version uses a smaller volume magnet than the typical model, considering the price of the magnet. Also, SPMSM was selected for convenience of control and high efficiency [6, 7]. First models in this paper have basic structure that can be used commonly and offset version that can reduce torque ripple [8], and adopted Halbach structure that can achieve a high magnetic field per volume of magnet through a special flux angle, which can reduce size and cost [9]. Therefore, the design target specifications must be satisfied while reducing the volume of the magnet. In terms of motor design, controlling the offset and pole arc ratio (PAR) are important to decrease torque ripple. First, this study designs the shape of the SPMSM with torque ripple at the similar level of the reference model, and then it proceed with the design by adjusting the offset and PAR. Currently, a model with good torque ripple characteristics is selected, and the control characteristics of the motor are confirmed by checking the torque and current according to speed change through SVPWM control. This application-focused study presents a direct comparative analysis of three representative SPMSM designs and provides practical guidance for reducing torque ripple under the same rated output conditions. The final design achieves similar performance while using a smaller magnet volume than the typical reference model, considering its cost-effectiveness in automotive water pump applications.

2. Analysis and Optimization of Models according to Rotor Topology

2.1. Design requirements for a PMSM for water pumps

In previous study [5], it was designed as an IPMSM for water pumps with rated speed 2800 (RPM), output power 2.8 (kW) and torque ripple 3.11(%), and the volume of magnet is about 66,000 (mm^3) for reference's PMSM.

©The Korean Magnetics Society. All rights reserved.
*Corresponding author: Tel: +82-43-841-5148
Fax: +82-43-841-5140, e-mail: yspark@ut.ac.kr

© 2026 Journal of Magnetics

Table 1. Parameter and specification of analysis model.

Parameter	Unit	Value
Pole	-	10
Slot	-	12
Rated Power	kW	2.8
Rated Speed	rpm	2800
Rated Torque	Nm	9.5
Current Density	A/mm²	Under 5
Stator Outer Dia.	mm	146
Stator Inner Dia.	mm	89
Lamination Length	mm	49
Rated Voltage	V	594

Table 1 shows the parameters and specification of analysis model. This paper investigates a 10-pole-12-slot surface PMSM for water pumps. Rated speed is 2,800 (rpm), rated torque is 9.5 (Nm) and current density is less than 5(A/mm²) with natural cooling method [10]. The yellow line in Fig. 1 indicates the magnetization direction of the magnet. There are models Angular 15 version, Angular 15 with offset version and Halbach version that were interpreted first. From now on, in this paper, angular 15 version is defined as model A. Similarly, angular 15 with offset version is defined as model B while Halbach version is defined as model C, and final version is defined as model D. The magnetization direction of Fig. 1(a) and Fig. 1(b) is calculated as 90(deg.), and the magnetization direction of Fig. 1(c) is calculated as 90(deg.), 130(deg.), and 135(deg.), respectively. Offset structure starts from a circle 26(mm) from the origin, and the angle of the magnet starts at 15(deg.). The 3 types of structures are analyzed under no-load and load conditions through finite element analysis (FEA) to derive the results, and the offset and angle of the model with the best characteristics are selected again to proceed with the analysis.

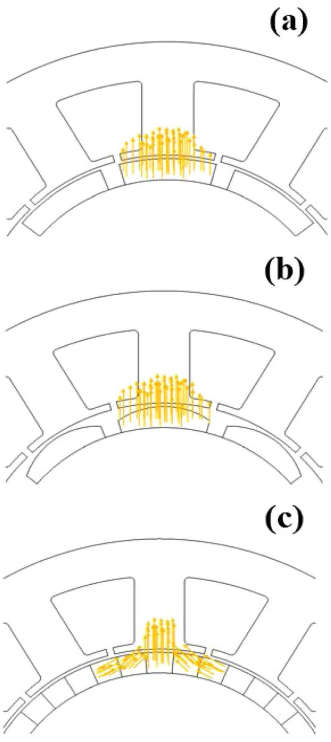

Fig. 1. (Color online) Comparison of 3Type Rotor magnetic flux direction: (a) Model A (typical) (b) Model B (offset) (c) Model C (Halbach).

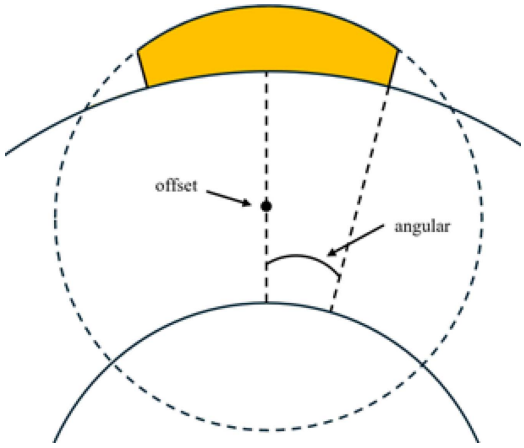

Fig. 2. (Color online) Calculation method of offset and angular.

In Fig. 2, offset in design refers to the distance from the origin to the center of the rotor, and angle refers to the angle of the magnet's cut from the vertical. Futhermore, the yellow part represents the area of the magnet. Therefore, the offset increases or the angle decreases while the area of the magnet decreases. This is used when calculating model A and model B.

2.2. Design and Physical properties information for PMSM

Fig. 3 is drawing of the mechanical design of PMSM. It shows the encoder, encoder zig, front cover, disk, rotor,

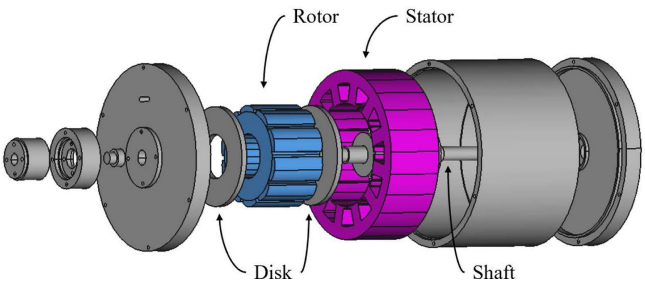

Fig. 3. (Color online) Mechanical design of rotor and stator.

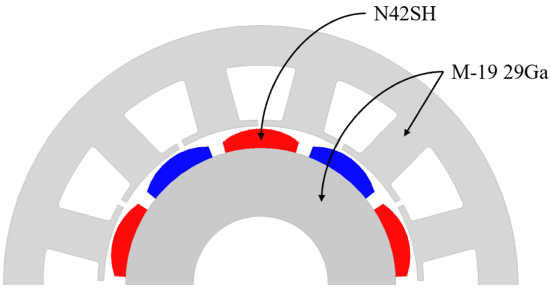

Fig. 4. (Color online) Material information of Rotor and Stator.

stator, bearing, shaft, housing and back cover in order from the left. Fig. 4 is material information of magnetic and iron core.

At first, M-19 29Ga is a non-oriented silicon steel, and this material is one of the materials frequently used in PMSM because of its high torque density [11]. In addition, N42SH is a neodymium series magnet, and it is widely used due to its high magnetic flux density.

Table 2 and Table 3 show the B-H curve of N42SH and M-19 29Ga at 20(°C). In Table 2, saturation and demagnetization occur when B_r is approximately 1.3(T) or higher and H_{cj} is 955,000 (A/m) or higher, respectively. Additionally, Table 3 indicates the specification of M-19 29Ga at 20(°C). Saturation occurs over 2.5(T) and demagnetization occurs over 330,000 (A/m). And all designs use NdFeB N42SH magnets, and the magnet properties are taken directly from the supplier's catalog nominal values at 20°C and used unchanged in the FEA models. This ensures transparent, catalog-traceable inputs across all models.

2.3. Analysis model of three types PMSM

The THD can be derived by fundamental harmonic X_1, i_{th} harmonic X_i, and maximum harmonic order as shown in (1) [12]. In this study, the maximum harmonic order was determined as 9 for convenience in that more harmonic orders can be neglected.

Table 2. Specification of N42SH magnet model.

Specification	B_r	H_{cb}	H_{cj}	$(BH)_{max}$	T_w
Unit	T	A/m	A/m	J/m^3	° C
Value	1.3	955000	1592000	330000	150

Table 3. Specification of M-19 29Ga model.

Specification	B	H	T
Unit	T	A/m	° C
Value	2.5	330000	20

Table 4. Specification of 3type rotor magnetic model.

Parameter	Unit	Model A	Model B	Model C
Magnet volume	mm^3	56,272	48,060	67,500
Efficiency	%	96.64	96.61	96.80
Torque Ripple	%	11.96	2.72	9.61
Total Torque	Nm	10.83	9.75	10.88
Output Power	W	3176.43	2861.72	3190.95
Total Loss	W	43.93	36.57	44.31
Back-EMF THD	%	9.3	9.8	9.6

$$THD = \sqrt{\sum_{i=2}^{K} \frac{X_i^2}{X_1^2}} \times 100 \tag{1}$$

Table 4 shows the main specifications of the three models. While the efficiency of all 3 models' characteristics is similar, the torque ripple of model B was the best among the 3 initial models at 2.7 (%). Total torque is similar for the model A and the model C at 10.8 (Nm), and the torque of the model B is 9.8 (Nm). THD was confirmed to be the best in model A at 9.3 (%). In addition, the total loss was confirmed to be the best in model B with the lowest result. Table 4 also shows information on magnet volume. It is important to compare the volume of magnets to design a machine that produces the same level of torque and output while reducing the amount of magnets used. In reference, magnet volume in PMSM was about 66000 (mm^3). Model A shows good results by using 56727 (mm^3), which is 16.3(%) less than the existing model, and model B shows good results by using 48060 (mm^3), which is 37.3(%) less than the reference model. On the other hand, magnet volume of model C is about 2.2(%) more and use 67500 (mm^3). And Model C, which has a similar volume to the existing reference, shows a torque of 10.8 (Nm), and shows the same torque value as Model A, which has a reduced volume compared to the reference. Since the volume is judged to be large compared to the torque, no additional design is performed.

The torque is determined by equation (2). Total torque is sum of magnetic torque and reluctance torque.

$$T = T_m + T_r = \frac{3}{2}\frac{P}{2}\left[\lambda i_q + (L_d - L_q) i_d i_q\right] \tag{2}$$

Where, T_m is the magnetic torque; T_r is the reluctance torque; P is the pole pairs; λ is the flux linkage; i_d is the direct-axis current; i_q is the quadrature-axis current; L_d is the direct-axis inductance and L_q is the quadrature-axis inductance [13]. and Fig. 5 shows the comparison of 3

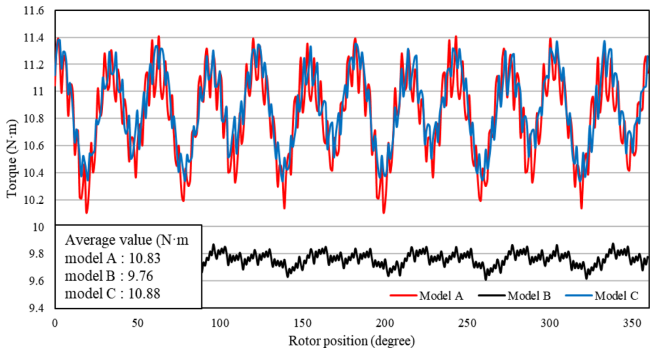

Fig. 5. (Color online) Comparison of three types of torque according to rotor position.

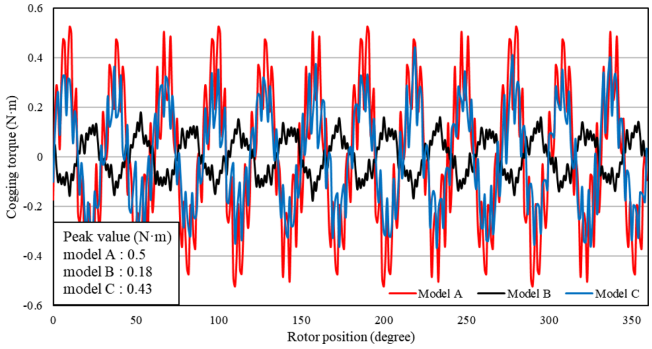

Fig. 6. (Color online) Comparison of 3 types of cogging torque.

types of torque models. Red line means model A's torque; black line shows model B's torque and blue line means model C's torque. Although the torque characteristics of model A and model C seem to be appropriate, the torque and torque ripple characteristics of model B are good, because the torque ripple value is about 7 to 9(%) larger than model B. Because the torque ripple is large, it can become unstable in many ways. Since the stator, windings, and volume are the same, the torque ripple is reduced by the shape of the magnet.

On the other hand, cogging torque is a factor that accounts for a large portion of torque ripple, and it is caused by the inter reaction of the magnetic flux by rotor magnet with irregular air gap [14]. To solve these problems, there are several ways to reduce cogging torque through design. Such as skew, adjusting the number of poles and slots, and pole arc ratio (PAR), but in this paper, we proceed with a design to reduce cogging torque by adjusting pole arc ration (PAR) to make unequal air-gap [15]. The cogging torque can be calculated by (3). Where W_c is the negative derivative of co-energy; α is the rotor position angle [16].

$$T_{cog}(\alpha) = -\frac{\partial W_c(\alpha)}{\partial \alpha} \tag{3}$$

Fig. 6 represents the no-load cogging torque. The colors are set as in Fig. 5. The size of the cogging torque of model B appears to be smaller than model A and model C. On the contrary, the cogging torque of model A showed the largest value, reaching up to 0.5~0.6 (Nm). Interpreting the above results, it can be seen that the torque ripple of model B, which has small cogging torque, is also small. Judging from the torque ripple and cogging torque, it can be seen that the rotor shape of model B is well designed.

Demagnetization can be caused by high temperature conditions, high external magnetic fields, or by the incorrect design of PM motors, which leads to performance degradation.

For these reasons, it is important to judge demagnetization and check their performance [17]. Fig. 7 is the

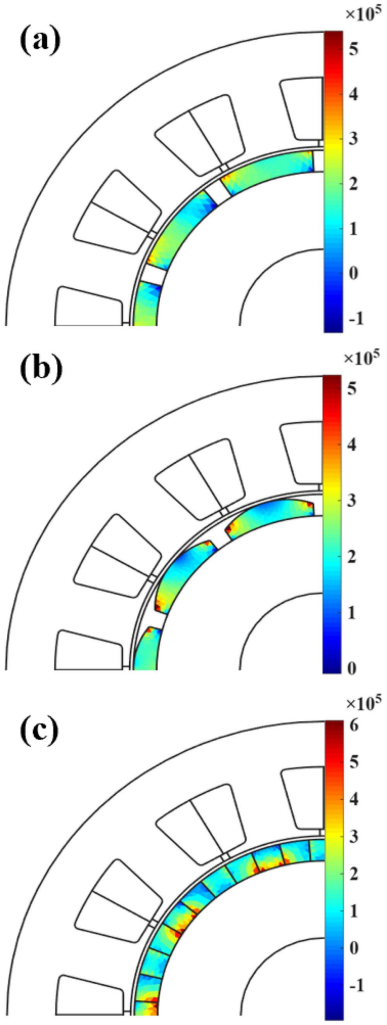

Fig. 7. (Color online) Irreversible Demagnetizing Field of 3types of rotor design. (a) Model A, (b) Model B, (c) Model C.

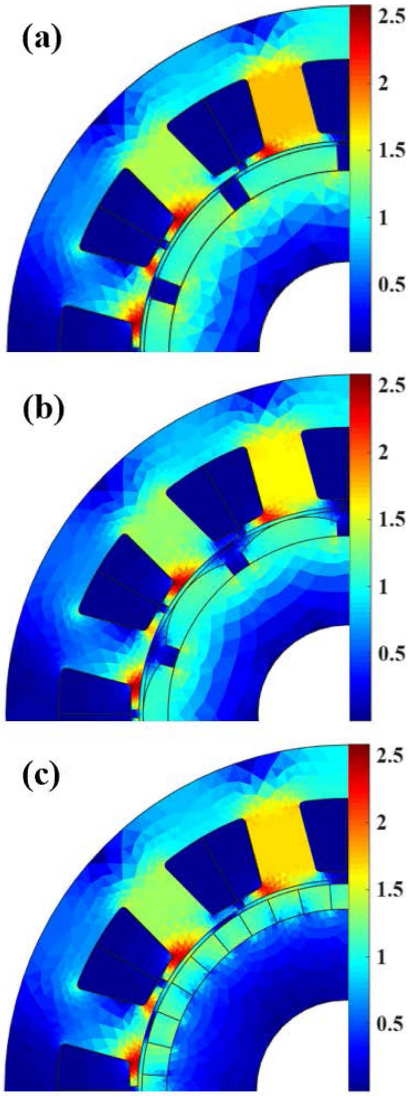

Fig. 8. (Color online) Magnetic Flux Density comparison of three models. (a) Model A, (b) Model B, (c) Model C.

irreversible demagnetizing field occurring in the magnet of the rotor. In the structure of the continuous magnets in Fig. 7(c), saturation of up to 600 (kA/m) occurs. In Fig. 7(a) and Fig. 7(b), a demagnetization phenomenon of up to 500 (kA/m) occurs at the ends of the magnets. However, since Table 2 indicates that demagnetization occurs at 1.592 (kA/m), it is considered good value. Comparing the value of Table 2 with the value of the graph, all three models have good demagnetization characteristics.

Saturation at rotor core and stator core limits the performance of PMSM [18]. So, designing without saturation is one of the most important factors in motor design. Fig. 8 is a diagram showing the magnetic flux density distribution of the rotor and stator models. Although Fig. 8(c) has an overall higher flux density value than Fig. 8(a) and Fig. 8(b), because of the magnetization direction of the Halbach structure. However, in Fig. 8(a), Fig. 8(b), and Fig. 8(c), all have magnetic flux density values less than the maximum of 2.5 (T). Since Table 3 indicates that magnetic saturation occurs from 2.5 (T) or higher at 20(°C), it can be said that all three models have good magnetic saturation characteristics.

Iron loss is the main component of decreasing efficiency [19]. To make good characteristics, it is important to optimize the rotor shape to reduce harmonics [20]. Iron loss can be calculated like (4), and total iron losses are divided by hysteresis loss and eddy current loss. In

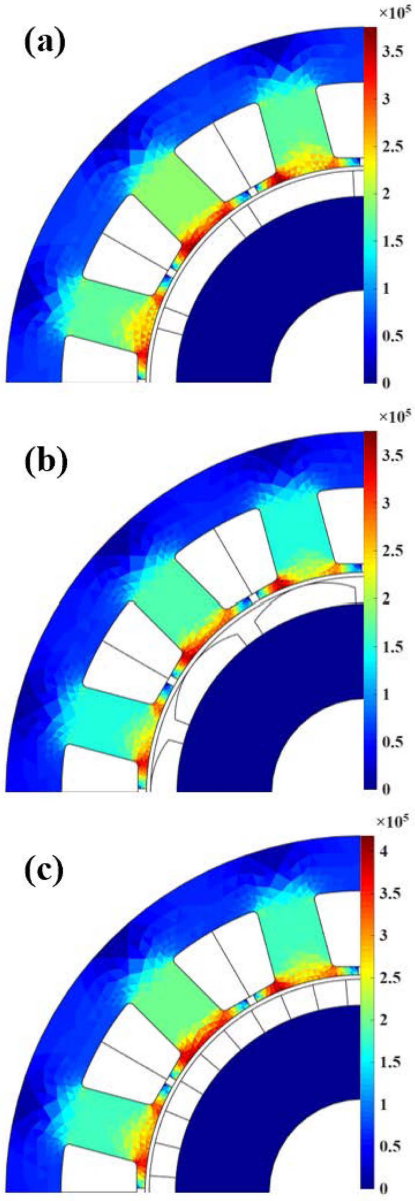

Fig. 9. (Color online) Iron Loss of three types model. (a) Model A, (b) Model B, (c) Model C.

hysteresis loss, where k_h is hysteresis loss coefficient; B_m is maximum flux density; n is Steinmetz coefficient; f is frequency; σ is eddy current loss coefficient [21].

$$P_i = P_h + P_e = k_h B_m^n f + \sigma_e (B_m f)^2 \quad (4)$$

Fig. 9 shows the iron losses of model A, model B and model C, respectively. In Table 2, it appears to be that the model B version has the lowest iron loss among the three models at 37(W). In the graph, the iron loss at the tooth of model A and model B is concentrated at a maximum of 350,000 (W/m^3), and the iron loss at model C is concentrated at a maximum of about 400,000 (W/m^3).

Efficiency is calculated in the form of dividing the output by the input. At this time, the input may be expressed as the sum of output and loss in (5) [22].

$$\eta = \frac{P_{out}}{P_{in}} = \frac{P_{out}}{P_{out} + P_{loss}} \quad (5)$$

Fig. 10 is the efficiency in acceleration conditions from 0 (rpm) to 200 (rpm), and Table 5 is the efficiency in acceleration conditions from 0 to 2800 (rpm). Looking at the efficiency according to the speed increase of the model C and model A, it can be seen that the efficiency characteristics are the same except for the error. However, looking at the efficiency graph and table of model B, it can see that it is about 2(%) lower. The efficiency above 200 (rpm) shows a difference of 1(%), and when the constant speed rotation starts at the rated speed of 2800 (rpm), the efficiency of model B is the highest. When considering various factors such as torque ripple characteristics, magnetic flux density, demagnetizing field, and efficiency characteristics, the offset angle is adjusted based on model B that has a clear difference in torque ripple characteristics and additional design is carried out. Fig. 11 shows the torque ripple characteristics according to the offset and angular. A total change of 5 degrees was made from angle 12 to 16 and offset 24 to 28. As shown in the graph, as the angle approaches 12 degrees, the torque ripple tends to increase. And the combination of angle 14 and offset 26 shows the lowest torque ripple. At the same time, as shown in Fig. 12, both the volume of the magnet and output decrease as the angle decreases and the offset increases. The output decreases, so considering the design requirements, the output power

Table 5. Comparison of Efficiency per speed.

Speed (RPM)	Efficiency (%)		
	Model A	Model B	Model C
50	49.11	46.63	49.34
100	65.87	63.60	66.08
150	74.33	72.39	74.50
200	79.42	77.75	79.57
2800	98.18	98.19	97.99

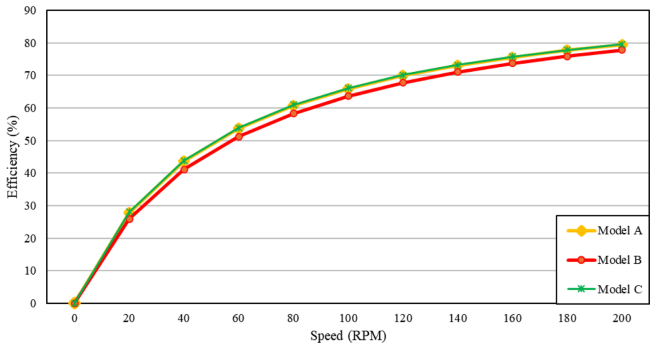

Fig. 10. (Color online) Efficiency comparison of three types model per speed.

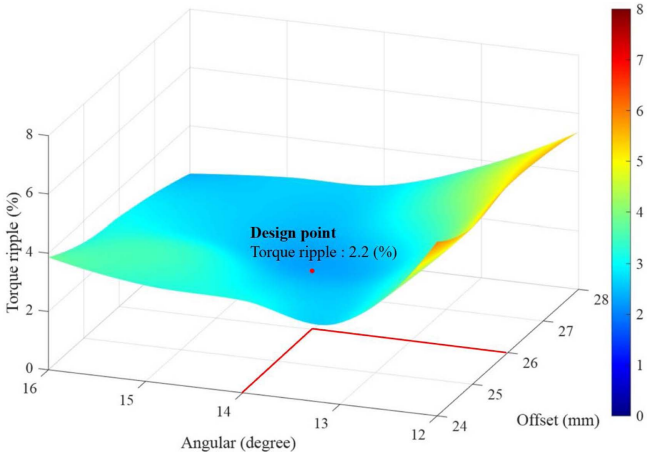

Fig. 11. (Color online) Torque ripple according to angle and offset position.

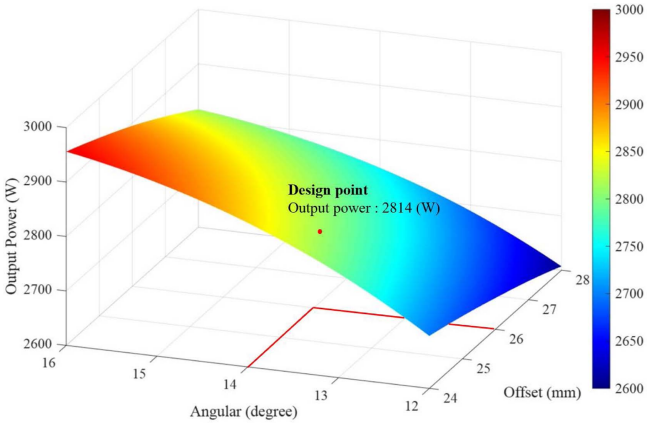

Fig. 12. (Color online) Output power.

value is 2.8 (kW) at angular 14 and offset 26, which is a suitable value. Furthermore, Fig. 13 shows the iron loss as the offset of the magnet increases. Iron loss, like output, tends to increase as the volume of the magnet increases. The iron loss of the angle 14 and offset 25 versions derived from Fig. 11 and Fig. 12 is measured to be approximately 35.5 (W). Fig. 14 is a graph showing the torque characteristics according to the angle and offset of the magnet. Considering torque ripple, output power, and iron loss, the 14-angle, 26-offset version demonstrates the favorable performance among the models capable of producing approximately 9.6 (Nm) of torque, thereby validating the effectiveness of the proposed design. And from now on, the angular 14 offset 26 version is defined as model D.

Fig. 15 shows the torque graph of model D. As the rotor rotates, torque changes, and the average torque value and torque ripple are calculated to be 9.5 (Nm) and 2.2(%), respectively, showing good characteristics. Fig. 16 shows the no-load back-EMF of model D. The no-load back-EMF is measured to be approximately 63 (V). Next, Fig. 17 is a graph analyzing the harmonic components of the torque of Model D. The 6th harmonic is confirmed to be approximately 0.002(%) of the total torque. In other words, it is determined that the harmonic component caused by the rotor does not affect the total torque ripple. When considered as a whole, this means that torque

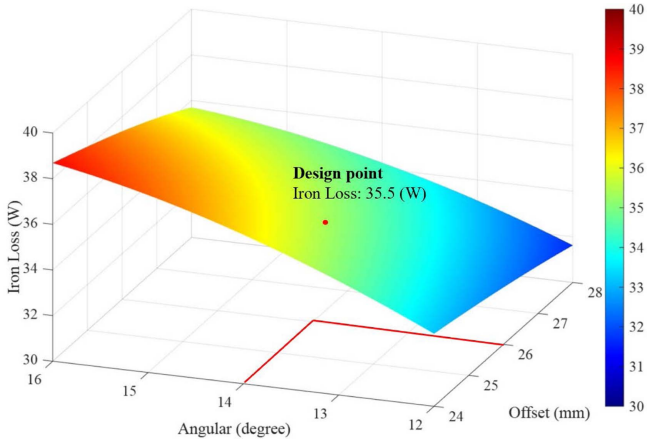

Fig. 13. (Color online) Iron loss variation according to angle and offset of permanent magnet in rotor.

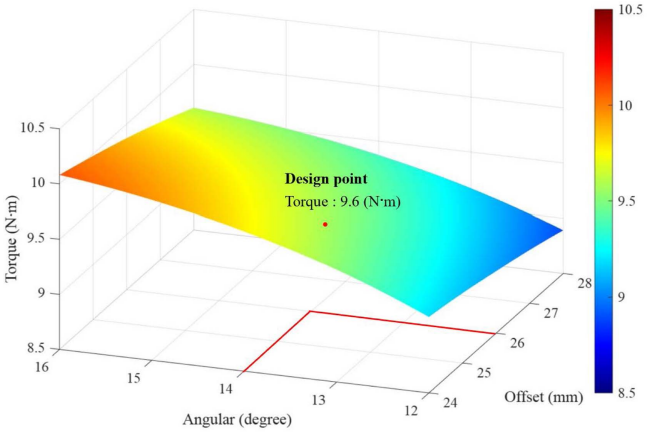

Fig. 14. (Color online) Comparison of torque according to angle and offset.

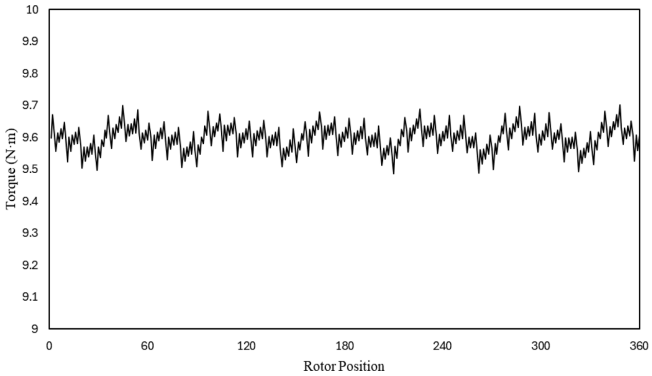

Fig. 15. (Color online) Torque change of model D.

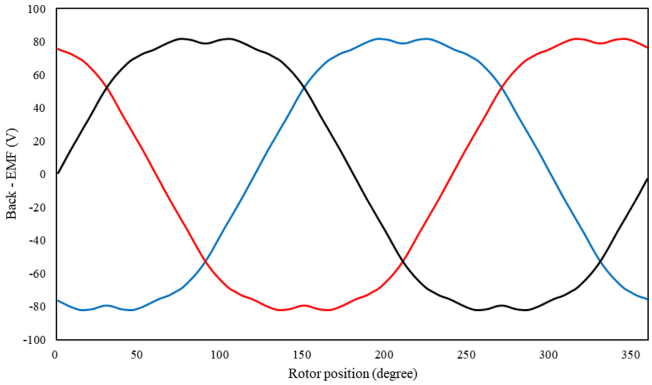

Fig. 16. (Color online) No-load three phase back-EMF.

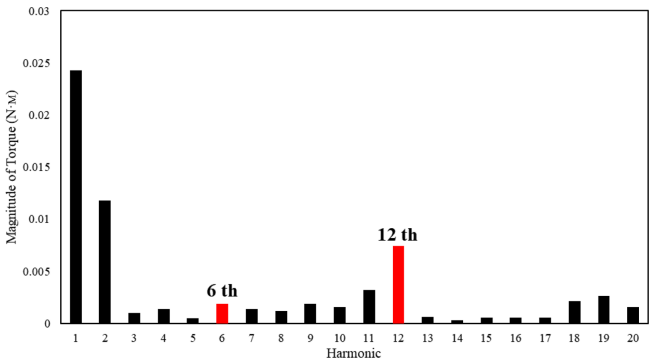

Fig. 17. (Color online) Harmonic component analysis of magnet flux of model D.

ripple was successfully reduced by adjusting the offset and angle of the rotor.

In Fig. 18, Winding copper loss can be calculated by (6). Winding copper loss is about loss within winding resistance and winding current.

$$P_{cu} = mI^2R \tag{6}$$

Where m is number of phases; I is the stator current; R is the resistance of stator [23]. Based on the geometric parameters shown in Fig. 19, the iron core loss can be calculated using (7). P_{Fe} means iron core loss; $P_{10/50}$ is the loss from silicon steel at 50 (Hz); m_i is the mass of iron; k is coefficient [23].

The eddy current loss is caused by rotate magnetic field. Where E is the strength of the eddy current field; J is current density; V_p is the volume of the permanent magnet in (8) [23].

$$P_{Fe} = P_{10/50}B^2(f/50)^{1.3}\mathrm{m}_i\mathrm{k} \tag{7}$$

$$P_{eddy} = \int_{V_P} EJ_P dv_e = \int_{V_P} \frac{J_P^2}{\sigma} dv_e = \int_{V_P} \rho J^2 dv_e \tag{8}$$

Furthermore, the magnetic stability was examined to ensure safe operation. Figs. 20 and 21 present the on-load irreversible demagnetization and magnetic flux density of Model D, respectively. Considering the results presented in Figs. 18, 19, 20, and 21, the electromagnetic design meets the required performance criteria. And Fig. 22 shows the control characteristics of model D according to the reference speed. The maximum value during control was 2832 (rpm), and the error was approximately 1.1(%), indicating good control characteristics. I_d, I_q represent the D-axis current and Q-axis current of PMSM and are expressed as follows in (9) and (10) [24].

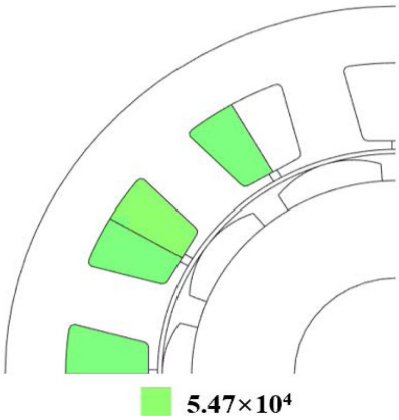

Fig. 18. (Color online) Joule loss density.

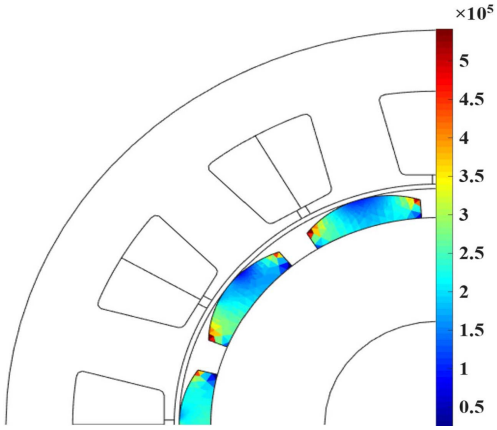

Fig. 20. (Color online) On-Load condition irreversible demagnetizing field of model D.

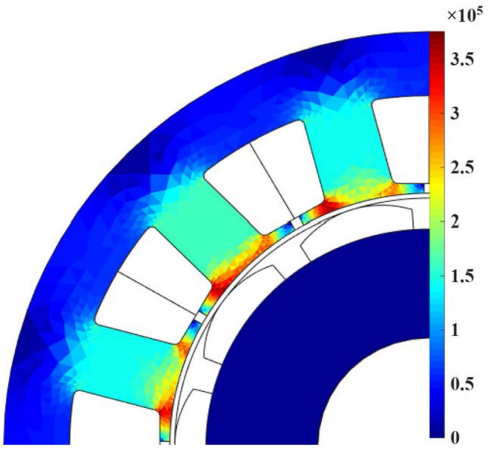

Fig. 19. (Color online) On-Load condition Iron loss of model D.

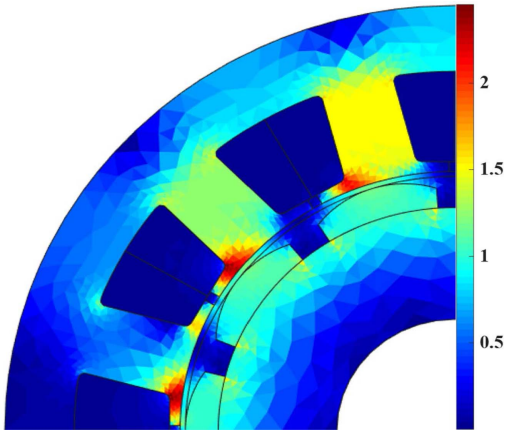

Fig. 21. (Color online) On-Load condition magnetic Flux Density of model D.

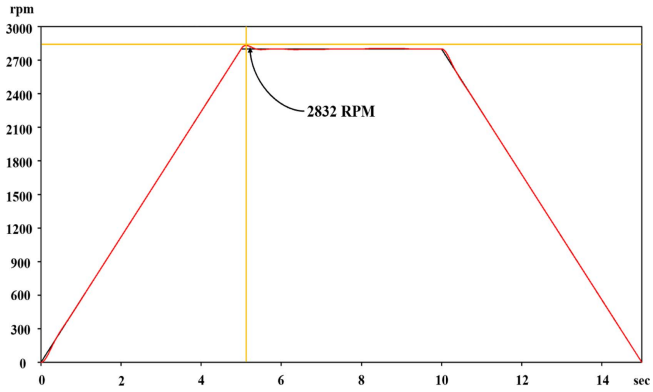

Fig. 22. (Color online) SVPWM speed control graph of model D.

$$\frac{di_d}{dt} = \frac{1}{L_d} v_d - \frac{R}{L_d} i_d + \frac{L_q}{L_d} i_q \omega_e \tag{9}$$

$$\frac{di_q}{dt} = \frac{1}{L_q} v_q - \frac{R}{L_q} i_q - \frac{L_d}{L_1} i_d \omega_e - \frac{\omega_e \psi f}{L_q} \tag{10}$$

In this model, V_d and V_q are D-axis voltage, Q-axis voltage; L_d and L_q are D-axis and Q-axis inductance; ω_e is electrical angular velocity.

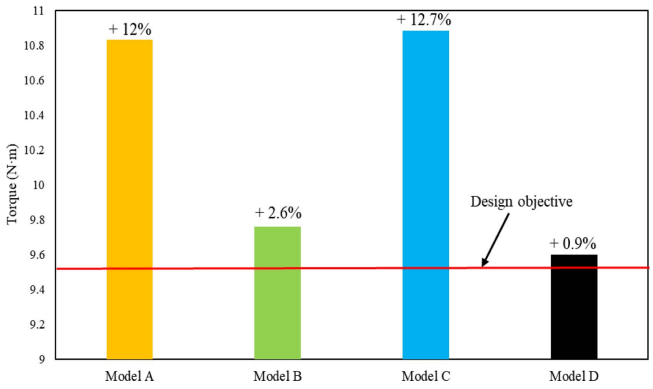

Fig. 23. (Color online) Torque comparison of 4 types of rotors.

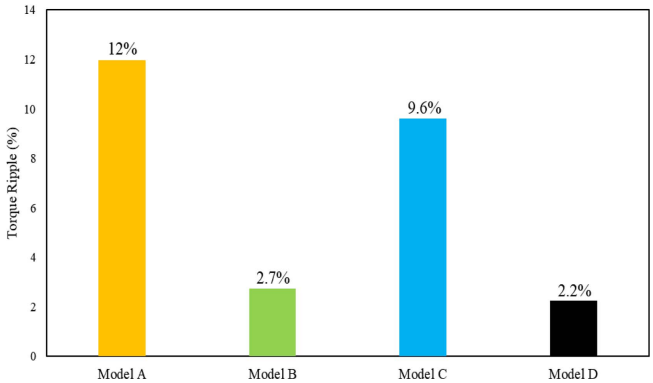

Fig. 24. (Color online) Torque Ripple Comparison of 4 types of rotors.

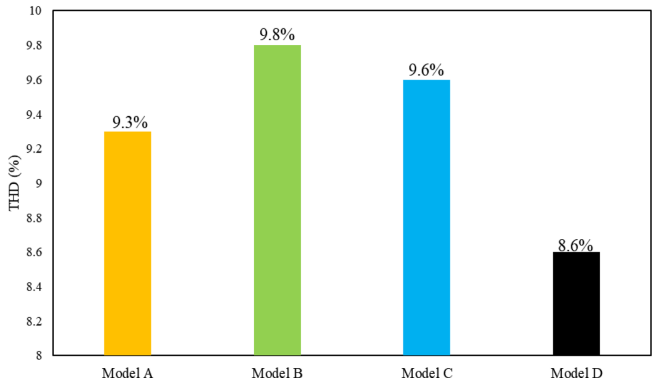

Fig. 25. (Color online) Comparison of 4 types of THD.

Fig. 23 is a graph comparing the torque from the initial three versions to the model D. The design target of 9.5 (N·m) must be satisfied, but the model C and model B show values exceeding the design target specification by 8.1(%) and 7.7(%), respectively. Model B shows the closest value with a 2.5(%) error from the design target specification, and model D also shows good values. Fig. 24 shows the torque ripple characteristics of four models, with model A and model C showing high values close to 10(%), and model D showing the best characteristics with a torque ripple of 2.2(%). Fig. 25 presents the THD analysis of the four models. Among them, Model D exhibited the lowest THD of approximately 8.6(%), demonstrating superior performance.

3. Conclusion

This study proposed a motor design with the best characteristics through the process of designing and optimizing three types of representative rotor structures of permanent magnet synchronous motors for water pumps. We designed the initial version that included typical version, pole arc ratio (PAR) adopted version and Halbach version. Among them, we conducted additional design of the offset version, which has good torque, output, and torque ripple characteristics. Using a local 5×5 grid around the baseline, we identified a design that meets the rated output while minimizing torque ripple, capturing the interactions between offset and angle. As a result, model D uses a total magnet volume of 45,864 (mm^3), which is 23.7(%) less than the basic version, model A. In addition, the volume of the magnet was reduced by approximately 4.8(%) compared to model B, which has the same offset applied, and by 47(%) compared to model C, which is a reduced version.

In addition, THD also shows a smaller value of 8.6(%)

than the three existing models, and the torque is also closest to the design target specification of 9.5 (N·m), indicating that the design was performed most satisfactorily.

Acknowledgment

This was supported by Korea National University of Transportation in 2026.

References

[1] J. H. Choi, Y. D. Chun, P. W. Han, M. J. Kim, D. H. Koo, J. Lee, and J. S. Chun, IEEE Trans. Magn. **46**, 3701 (2010).
[2] H. Ying, S. Huang, and D. Xu, CES Trans. Elec. Mach. and Sys. **1**, 354 (2017).
[3] N. Bianchi, E. Fornasiero, and W. Soong, IEEE Trans. Ind. Appl. **51**, 3600 (2015).
[4] M. Onsal, Y. Demir, and M. Aydin, IEEE Trans. Magn. **53**, 8700606 (2017).
[5] W. Pei, P. Xiao, J. Pan, Z. Li, and A. Lv, MDPI Appl. Sci. **14**, 9666 (2024).
[6] Y. Wan, S. Wu, and S. Cui, IEEE Trans. Appl. Supercond. **26**, 0608405 (2016).
[7] B. Wang, Y. Shao, Y. Yu, Q. Dong, Z. Yun, and D. Xu, IEEE Trans. Power Elec. **36**, 11910 (2021).
[8] D. Wu and Z. Q. Zhu, IEEE Trans. Magn. **51**, 8108704 (2015).
[9] S. Wu, S. Cui, and W. Zhao, IEEE Trans. Plas. Sci. **43**, 91 (2025).
[10] L. Boscaglia, H. S. N. Sugumar, N. Sharma, and Y. Liu, IEEE Trans. Transpor. Elec. **11**, 236 (2025).
[11] Y. Li, C. Yan, S. Xie, L. Zeng, and R. Pei, IEEE Trans. Magn. **60**, 2001305 (2024).
[12] Y. Du, T. Tao, W. Zhao, J. Ji, and Z. Li, IEEE Trans. Transpor. Elec. **10**, 1377 (2015).
[13] S. U. Chung, S. H. Moon, D. J. Kim, and J. M. Kim, IEEE Trans. Ind. Elec. **63**, 302 (2016).
[14] Jacek F. Gieras, IEEE Trans. Ind. Appl. **40**, 1310 (2004).
[15] M. Aydin and M. Gulec, IEEE Trans. Ind. Elec. **61**, 5025 (2014).
[16] P. Wang, Z. Zhang, C. Liao, J. Li, and X. Xie, IEEE Trans. Ind. Appl. **61**, 2934 (2025).
[17] F. Mahmouditabar, A. Vahedi, and F. Marignetti, IEEE Acc. **11**, 47750 (2023).
[18] S. Fang, H. Liu, H. Wang, H. Yang, and H. Lin, IEEE Trans. Appl. Supercond. **29**, 0602805 (2019).
[19] A. Balamurali, A. Kundu, Z. Li, and N. C. Kar, IEEE Trans. Ind. Appl. **57**, 363 (2021).
[20] F. Chai, P. Liang, Y. Pei, and S. Cheng, IEEE Trans. Magn. **51**, 6301404 (2015).
[21] D. J. Kim, D. K. Hong, J. H. Choi, Y. D. Chun, B. C. Woo, and D. H. Koo, IEEE Trans. Magn. **49**, 2319 (2013).
[22] H. Zhang and D. Xiao, IEEE Trans. Circ. and Sys. **71**, 4924 (2024).
[23] D. Tan, F. Qiu, H. Han, and Z. Pang, IEEE/ASME Trans. Mech. **10**, 4755 (2024).
[24] Z. Li, F. Wang, D. Ke, J. Li, and W. Zhang, IEEE Trans. Power Elec. **36**, 14398 (2021).